SPECIAL TOPIC

# Microstructure evolution of T91 steel after heavy ion irradiation at 550 °C*

SPECIAL TOPIC — Ion beam modification of materials and applications

# Microstructure evolution of T91 steel after heavy ion irradiation at 550 °C*

Ligang Song(宋力刚)[1], Bo Huang(黄波)[1], Jianghua Li(李江华)[2], Xianfeng Ma(马显锋)[1,†], Yang Li(李阳)[3,4,‡], Zehua Fang(方泽华)[1], Min Liu(刘敏)[1], Jishen Jiang(蒋季伸)[1], and Yanying Hu(胡琰莹)[1]

[1] *Sino-French Institute of Nuclear Engineering and Technology, Sun Yat-Sen University, Zhuhai* 519082, *China*
[2] *State Key Laboratory of Nonlinear Mechanics (LNM), Institute of Mechanics, Chinese Academy of Sciences, Beijing* 100190, *China*
[3] *DEN-Service de Recherches Métallurgiques Appliquées, CEA, Université Paris-Saclay, Gif-sur-Yvette* 91191, *France*
[4] *Department of Mechanical and Aerospace Engineering, University of California Los Angeles, Los Angeles, CA* 90095, *USA*

(Received 30 March 2021; revised manuscript received 5 June 2021; accepted manuscript online 11 June 2021)

Fe-Cr ferritic/martensitic (F/M) steels have been proposed as one of the candidate materials for the Generation IV nuclear technologies. In this study, a widely-used ferritic/martensitic steel, T91 steel, was irradiated by 196-MeV $Kr^+$ ions at 550 °C. To reveal the irradiation mechanism, the microstructure evolution of irradiated T91 steel was studied in details by transmission electron microscope (TEM). With increasing dose, the defects gradually changed from black dots to dislocation loops, and further to form dislocation walls near grain boundaries due to the production of a large number of dislocations. When many dislocation loops of primary $a_0/2\langle 111\rangle$ type with high migration interacted with other defects or carbon atoms, it led to the production of dislocation segments and other dislocation loops of $a_0\langle 100\rangle$ type. Lots of defects accumulated near grain boundaries in the irradiated area, especially in the high-dose area. The grain boundaries of martensite laths acted as important sinks of irradiation defects in T91. Elevated temperature facilitated the migration of defects, leading to the accumulation of defects near the grain boundaries of martensite laths.

**Keywords:** T91 steel, high energy Kr ions irradiation, irradiation defects, transmission electron microscope (TEM)

**PACS:** 61.82.–d, 61.72.U–, 61.72.–y, 07.78.+s **DOI:** 10.1088/1674-1056/ac0a64

## 1. Introduction

With the growing global demand for clean and safe energy, there is an increasing interest in the Generation IV nuclear technologies. The development of new nuclear reactors, nuclear power systems, and nuclear technical instruments also raises new security issues. Generally, the more hostile working environments than the current reactor systems require better system design, structure, safety evaluation, and assurance. One of the most significant challenges is finding suitable materials that can withstand the demanding operating conditions of higher temperature, higher neutron dose, more aggressive corrosion, and so on.[1–4]

Fe–Cr ferritic/martensitic (F/M) steels have been proposed as one of the candidate materials due to the good irradiation resistance, high temperature properties, high thermal conductivity, and low thermal expansion coefficient. Among them, T91 as a primary ferritic/martensitic steel, has been widely used as structural material in nuclear power components and investigated for tens of years around the world.[1,5–7] Especially, T91 steels exhibit high strength at elevated temperatures, good creep performance, good resistance to thermal fatigue, and corrosion as well.[8–10] It is important to understand the microstructural evolution of T91 steels at service environments to ensure the safety and reliability in future reactors. For instance, the irradiation would induce microstructural modifications of material, such as void, dislocation loops, defects, and so on, which would significantly change the mechanical properties of the material.

In recent years, increasing studies have been focused on the microstructural evolution and degradation mechanism of T91 steel under different irradiation conditions, such as various implanted ions, different irradiation temperatures, and irradiation dose. Yeli *et al.*[11] found that Mn, Ni, Si-rich (MNS-rich) clusters would form in T91 steel when irradiated to neutron doses between 14.6 dpa and 35.1 dpa in BOR60 reactor at temperatures between 376 °C and 415 °C. This phenomenon was not observed at higher temperatures of 460 °C and 524 °C. Van Renterghem *et al.*[12] studied the T91 steel samples irradiated with neutrons and protons to a cumulative dose of 0.88 dpa, 2.07 dpa, and 4.35 dpa at temperatures of

*Project supported by Guangdong Major Project of Basic and Applied Basic Research (Grant No. 2019B030302011), the National Natural Science Foundation of China (Grant Nos. U2032143, 11902370, and 52005523), the International Science and Technology Cooperation Program of Guangdong Province, China (Grant No. 2019A050510022), the China Postdoctoral Science Foundation (Grant Nos. 2019M653173 and 2019TQ0374), and the Heavy Ion Research Facility of Lanzhou (HIRFL).

†Corresponding author. E-mail: maxf6@mail.sysu.edu.cn
‡Corresponding author. E-mail: yang.li@cea.fr

 

254 °C, 260 °C, and 350 °C under transmission electron microscope (TEM). In all samples irradiated up to 1 dpa, irrespective of irradiation conditions, dislocation loops were segregated near the line dislocations, forming a heterogeneous distribution. On the other hand, in the high-dose sample, dislocation loops were uniformly distributed in the grain interior. And the middle-dose sample showed a mixed character. Jiao *et al.*[13] investigated the microstructures of T91 after neutron irradiation in the BOR60 reactor between 376 °C and 524 °C up to doses between 15.4 dpa and 35.1 dpa. Type $a\langle 100\rangle$ dislocation loops were observed at 376 °C–415 °C and network dislocations dominated at 460 °C and 524 °C. Cavities appeared in a bimodal distribution with a high density of small bubbles less than 2 nm at irradiation temperatures between 376 °C and 415 °C. Small bubbles were also observed at 460 °C and 524 °C but cavities greater than 2 nm were absent. Tan *et al.*[14] evaluated the irradiation resistance of T91 in the Advanced Test Reactor to 4.3 dpa at the working temperature of 469 °C. It showed that T91 had a high number density of dislocation loops and a low level of irradiation-induced segregation. Irradiation-induced cavities were observed in T91 but remained small, usually less than 10 nm.

Owing to the expensive cost and time consuming of neutron irradiation, ion irradiation has been often employed to induce irradiation damage in materials. Prasitthipayong *et al.*[1] investigated several candidate structural alloys for Gen-IV reactors (800H, T91, nanocrystalline T91 and 14YWT) which were irradiated with 70-MeV $Fe^{9+}$ ions at 452 °C to an average dose of 20.68 dpa. The T91 steel showed a higher ratio of edge dislocations. Zhu *et al.*[15] studied T91 steel irradiated by 1.625-MeV Fe ions to the fluence of $2.5\times10^{15}$ ions/cm$^2$ from room temperature (RT) to 550 °C and found that the sample irradiated at RT possessed the largest concentration of vacancy-type defects. At higher temperatures, the vacancy-type defects concentrations were in an increasing trend of 550 °C, 300 °C, 450 °C. Zhu *et al.*[16] investigated temperature-dependent surface modification induced in T91 steel irradiated by 3.25-MeV Fe-ions to fluence of $1.7\times10^{16}$ ions/cm$^2$ at room temperature, 300 °C and 450 °C, respectively. It was found that the concentration of open-volume defects in T91 samples decreased with increasing implantation temperature. By *in-situ* transmission electron microscopy (TEM), Zheng *et al.*[17] investigated the microstructural evolution of ferritic/martensitic (F/M) steel T91 irradiated to 4 dpa and 10 dpa at 470 °C using 1-MeV $Kr^{2+}$. The irradiated microstructure included primarily dislocation loops, in which the average size and density is a function of irradiation dose. Liu *et al.*[18] have studied the microstructural evolution of ferritic/martensitic steel T91 under 1-MeV Kr ion irradiation up to $4.2\times10^{15}$ ions/cm$^2$ at 300 °C, 400 °C, and 500 °C. At 300 °C, grown-in defects are strongly modified by black dot loops, and dislocation networks together with black-dot loops were observed after irradiation. At 400 °C and 500 °C, grown-in defects are only partially modified by dislocation loops; isolated loops and dislocation segments were commonly found after irradiation. About 51% of the loops were $a_0/2\langle 111\rangle$ type for the 400-°C irradiation, and the dominant loop type was $a_0\langle 100\rangle$ for the 500-°C irradiation.

It is seen from the previous studies that it is important to study the irradiation damage mechanism of T91 especially at high irradiation dose, *e.g.* up to 30 dpa, which has been rarely reported before. Besides, owing to the power of ion accelerators, the irradiated depths in T91 steels in previous studies were usually on the order of several micrometers, which limit the understanding of the bulk effects of irradiation damage. In this study, a ferritic/martensitic T91 steel were specially irradiated by 196-MeV $Kr^+$ ions up to 30 dpa at 550 °C, with an irradiation depth as large as 12 μm. By detailed TEM investigations of microstructure evolution related to irradiation at different depth, the primary-irradiated microstructural features and underlying mechanisms were disclosed and discussed.

## 2. Materials and experimental procedure

### 2.1. Materials

The chemical composition of as-received T91 steel is listed in Table 1. The T91 steel was normalized at 1045 °C for 10 min followed by air cooling, and then tempered at 780 °C for 1 hour followed by air cooling. A 10 mm×10×1 mm as-received T91 plate was cut by electrical discharge machining. The plate was mechanically ground with silicon carbide papers, and then eletropolished using 10% perchloric acid and 90% ethyl alcohol.

**Table 1.** The chemical composition (in unit wt%) of as-received T91 steel.

| Fe | Cr | C | Mn | Mo | Nb | Al | Cu | V | Si | Ni | N | S | P |
|---|---|---|---|---|---|---|---|---|---|---|---|---|---|
| Bal. | 8.53 | 0.1 | 0.4 | 0.15 | 0.076 | 0.01 | 0.022 | 0.21 | 0.38 | 0.12 | 0.05 | 0.001 | 0.015 |

### 2.2. Ion irradiation

The irradiation experiment was performed at the Institute of Modern Physics, Chinese Academy of Sciences, by use of the "Stress Materials Research Terminal" of Heavy Ion Research Facility of Lanzhou (HIRFL). The polished T91 specimen was irradiated by 196-MeV $Kr^+$ ions at 550 °C. Two sets of magnets were used to scan the ion beam with an area of 15 mm×15 mm during the ion beam bombard-

ing on the specimen to obtain a relatively uniform distribution in the irradiation dose. In the experiment, the beam intensity is not more than 3 μA to avoid the heating effect of ion beam during irradiation. The irradiation fluence reaches up to $2.4\times10^{16}$ ions/cm$^2$. In addition, the temperature was regulated based on the feedback from a K-type thermocouple attached to the specimen. By SRIM-2008 Kinchin–Pease quick calculation[19] is shown in Fig. 1. A displacement energy of 40 eV is considered for major elements such as Fe and Cr, while 25 eV is considered for C and N elements. Kr concentration distribution is over 10 μm to 12 μm damage depth from surface. The damage peak position is located at ~ 11-μm depth from surface and the value of peak damage is about 30 displacement per atom (dpa). The peak damage dose rate is $1.6\times10^{-4}$ dpa/s for the current irradiation. Below the depth of 10 μm, the ratio of Kr concentration to dpa is nearly zero. It is indicated that there is no significant effect of Kr atoms ranging from surface to 10 μm.

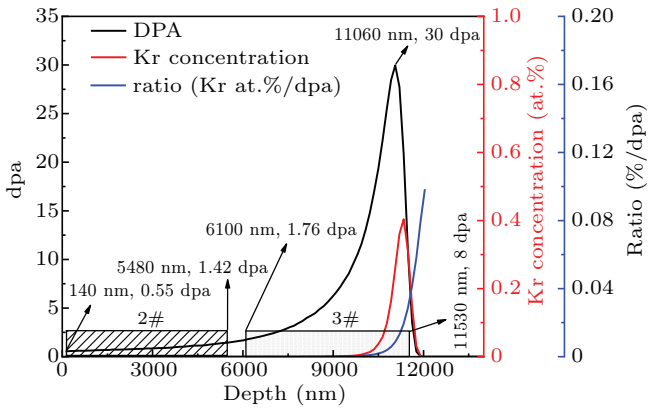


**Fig. 1.** The damage level, Kr concentration and ratio of concentration to dpa in Kr-irradiated T91 sample simulated by SRIM-2008. Then the irradiation sample of TEM is fabricated into two regions 2# and 3#.

### 2.3. Microstructure characterization

TEM analyses were carried out on an FEI Talos 200X TEM microscope to study the microstructural features and damage accumulation after irradiation. The TEM samples were fabricated by focused ion beam (FIB) lift-out technique with an FEI Quanta three-dimensional (3D) FEG dual beam scanning electron microscopy. In order to reduce contingent artefacts and obtain fine surface on FIB cross-section plane, a platinum (Pt) layer was deposited to protect the surface from ion damaging, and then the sample was milled from both sides to the final thickness of approximately 55 nm with the lowest possible current beam. The origin sample is fabricated as 1# shown in Fig. 2. To investigate the whole area from surface to the maximum irradiation depth of about 12 μm, the TEM samples were prepared from two parts, respectively. As shown in Fig. 2, one is from the surface to ~ 6-μm depth (2#), and the other is from about 6.1-μm to ~ 12-μm depth (3#). The irradiation damage can be predicated by SRIM, as shown in Fig. 1.

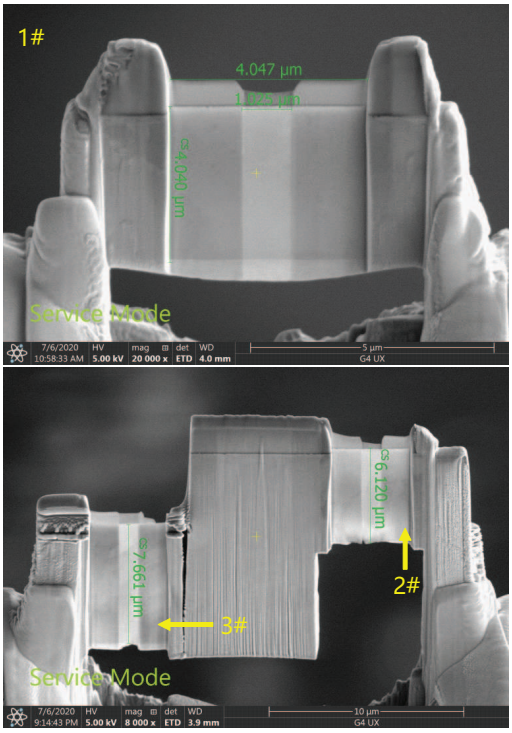


**Fig. 2.** The TEM sample fabricated by FIB. The origin sample is represented as 1#. The irradiation sample is divided into two parts, 2# from surface to ~ 6 μm and 3# from 6.1 μm to ~ 12 μm depth.

## 3. Results and discussion

### 3.1. Microstructure of as-received T91 steel

In Fig. 3, there are dislocations in some grains and a small amount of precipitates which are mainly formed at grain boundaries except some small size precipitates in the as-received T91 samples. By electronic diffraction spectroscopy (EDS), the composition (in unit at.%) of precipitates in the as-received T91 steel is shown in Table 2. The precipitates found in the unirradiated T91 steel were identified as $M_{23}C_6$ carbide-type precipitates. The coarser (0.1 μm–0.3 μm in length) $M_{23}C_6$ precipitates were usually along prior austenite grain boundaries (PAGB) and along subgrain boundaries.[20,21] A tempered martensitic microstructure being composed of packets and blocks of laths within prior-austenite grains, together with different precipitates formed at a variety of boundaries and matrix. By approximate calculation, the average size and density of precipitates is 155.2 nm and $2.43\times10^{21}$/m$^3$.

There are some black dots in deep layer, which might be introduced in the FIB preparation process. By estimation, the number density of black dots is about $2.5\times10^{21}$/m$^3$ with average size of 2.6 nm. Evidently, the initial dislocations are mainly restricted by grain boundaries because grain boundaries can act as strong sinks for defects.

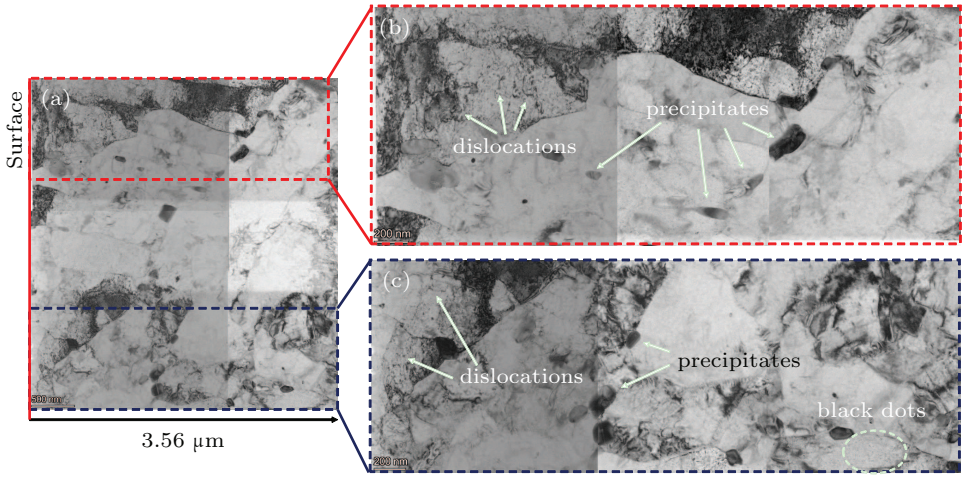


**Fig. 3.** TEM images of as-received T91 steel (a) and corresponding high-magnification images (b) and (c).

**Table 2.** The chemical compositions (in unit at.%) of the precipitates in T91 steel indicated by EDS.

| Region | Fe | Cr | Mo | C |
|---|---|---|---|---|
| Precipitate | 24.6–25.3 | 42.2–46.3 | 3.17–4.06 | 25.1–29.4 |

### 3.2. Microstructure of T91 after irradiation

In Fig. 4, from the SRIM results, the irradiation damage is below 1.7 dpa from surface to ∼ 6 μm. It is found that high density dislocations, dislocation loops and black dots aggregate to the grain boundaries. As the depth increases, the irradiation damage increased from 0.55 dpa to 1.42 dpa.

There are precipitates near grain boundaries with average size of 186.3 nm and the average number density of $3.55\times10^{19}$ m$^{-3}$, which is larger than that in T91 origin steel. The irradiation enhanced the growth of precipitates due to irradiation-assisted diffusion.[22] In low dose area, the irradiation would promote nucleation and growth of precipitates.

With increasing depth thus higher irradiation damage, the black dots are unobserved. Owning to the elevated temperature, the small size defects such as black dots would be easily to grow up to big size defects or migrate and subsequently interact with other defects. The density and average size of black dots marked by white arrows are about $6\times10^{21}$ cm$^{-2}$ and 3.6 nm, respectively. The results are slightly larger than T91 origin sample. The effect of FIB sample preparation process on black dots cannot be completely ignored. In addition, there are some dislocation segments which would due to the interactions of these black dots with dislocations.[18]

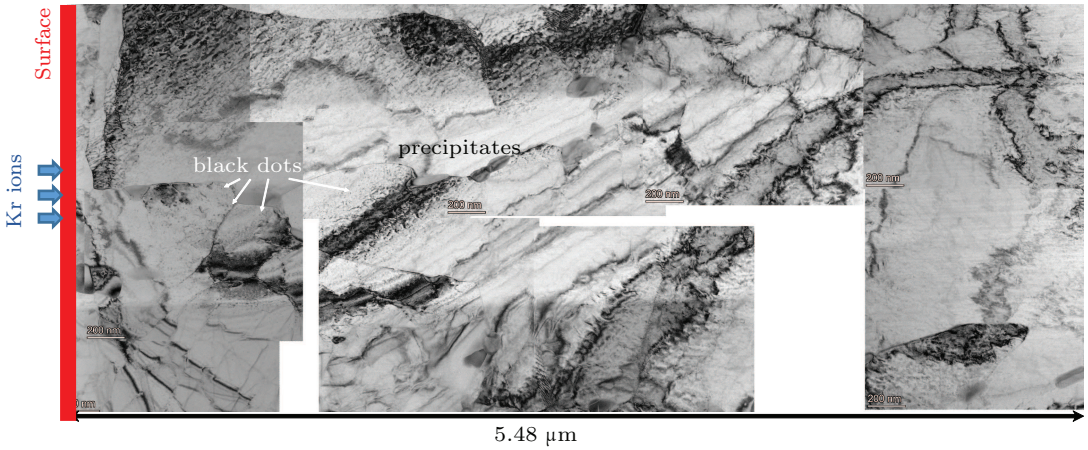


**Fig. 4.** TEM bright field image from surface to ∼ 6 μm of T91 irradiated by 196-MeV $Kr^+$ ions.

To study the features of irradiation defects, three grains at different depths were selected for investigation, in which the specimen was tilted near the [001] zone axis and only the specific $g$ vector image was strongly excited. The bright and dark field images of grains are shown in Fig. 5. Three selected areas shown in Figs. 5(a), 5(d), and 5(g) are located at the depth of 961 nm, 1148 nm, and 5121 nm, respectively. According the SRIM results, the corresponding irradiation damage are 0.63 dpa, 0.67 dpa, and 1.33 dpa, respectively. The type of vectors of dislocation loops produced by irradiation in Kr-irradiated T91 samples were believed as $a_0\langle100\rangle$ or $a_0/2\langle111\rangle$ type.[13,18] Figures 5(b), 5(c); 5(e), 5(f); and 5(h), 5(i) display the same region with different $\boldsymbol{g}$ vectors, respectively. In Figs. 5(b), 5(e), and 5(i), black dots and dislocations are all ob-

servable with a $\boldsymbol{g}$ vector of $\langle 110\rangle$, which are different from that in Figs. 5(c), 5(f), and 5(h). The contrast of dislocation loops is expected to vanish or become faint under diffraction condition while $\boldsymbol{g}\cdot\boldsymbol{b}=0$. Therefore, the Burgers vector of dislocation loops can be determined by the standard $\boldsymbol{g}\cdot\boldsymbol{b}$ analysis and comparing the orientation of the loops with the corresponding diffraction pattern. For example, when only $\boldsymbol{g}=200$ was strongly activated, only and $a_0[010]$, $a_0[001]$ loops would be absent ($\boldsymbol{g}\cdot\boldsymbol{b}=0$) and all other types of $a_0[100]$ and $a_0/2\langle 111\rangle$ loops are visible. When only $\boldsymbol{g}=1\bar{1}0$ was strongly activated, $a_0/2[111]$, $a_0/2[11\bar{1}]$ loops, $a_0[001]$ would be absent and $a_0[100]$, $a_0/2[1\bar{1}1]$, $a_0/2[1\bar{1}\bar{1}]$ loops are visible. Moreover, the dominant dislocation loop type in T91 under $Kr^+$ ion irradiation has been identified as $a_0\langle 100\rangle$ for irradiation at 470 °C and 500 °C.[17,18]

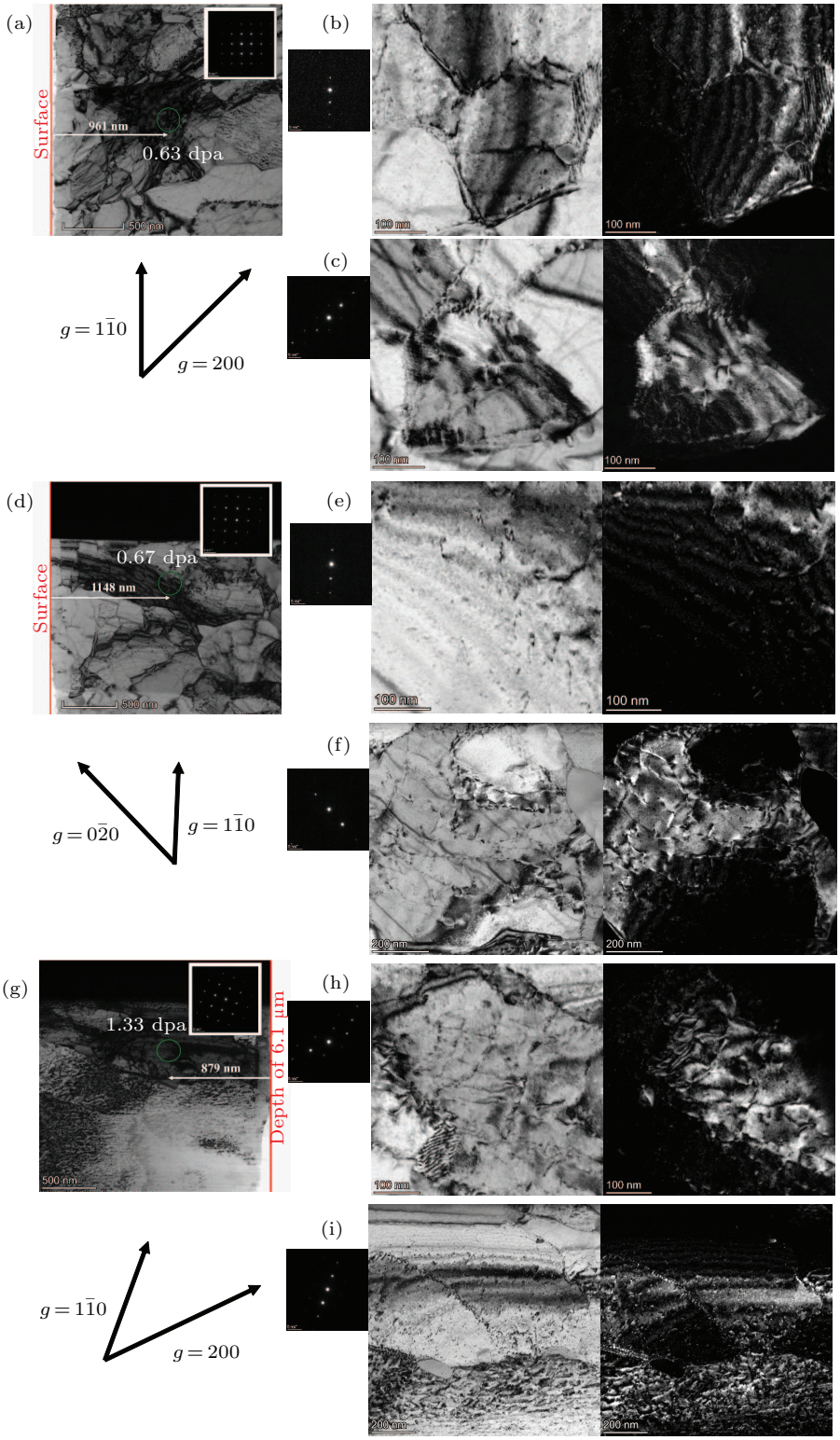


**Fig. 5.** Bright field and dark field TEM images of three areas with two different $\boldsymbol{g}$ vector $\langle 110\rangle$ and $\langle 200\rangle$ from surface to ~ 6 μm of T91 irradiated by $Kr^+$ ions.

There are some dislocation segments shown in Figs. 5(b) and 5(e). The $a_0/2\langle 111\rangle$ loops are highly mobile and $a_0\langle 100\rangle$ loops are sessile. Therefore, $a_0/2\langle 111\rangle$ loops can migrate over long distances and interact with distant grown-in defects, leading to formation of dislocation segments at lower dose, whereas $a_0\langle 100\rangle$ can only act as stationary defect sinks once formed.[18] Moreover, the complete $a_0\langle 100\rangle$ loops can also be generated from two interacting $a_0/2\langle 111\rangle$ loops.[23] In Figs. 5(b) and 5(e), the dislocation loops are few which would due to the annealing effect, more vacancies migrate and annihilate at defect sinks including interstitials, dislocations, dislocation loops, grain boundaries, and precipitates.[16] In addition, the annihilation of interstitial and vacancies at the line dislocations also explains the lower loop density noticed in irradiated sample with low irradiation damage.

With the depth increases, the defects gradually change from black dots to dislocation loops, and further form dislocation walls or gather around grain boundaries, as shown in Fig. 5(i). During this transition, part of grain boundaries continues to interact with defects, which would lead to the deformation of grain boundaries.

In Fig. 6, the peak damage (30 dpa) area is located at 11.06-μm deep and the minimum damage is 1.76 dpa (6.1-μm deep). Evidently, with higher irradiation damage, there are higher density dislocations in some grains, especially in the martensite laths. According to the bright field image and corresponding dark field image of orange and blue dashed line area, with higher irradiation damage, the high density dislocations become more unevenly distributed. The grain boundaries still restrict the distribution of dislocations. Near the grain boundaries, there are also amounts of precipitates with average size of 173.0 nm and average number density of $4.03\times10^{19}$ m$^{-3}$. Compared with the low dose area, the average size of precipitates increases but the density of precipitates decreases. The damage peak position predicted by SRIM did not show highest density of dislocations, which might be due to the trapping dislocation effects of martensite lath boundaries in T91 steel.

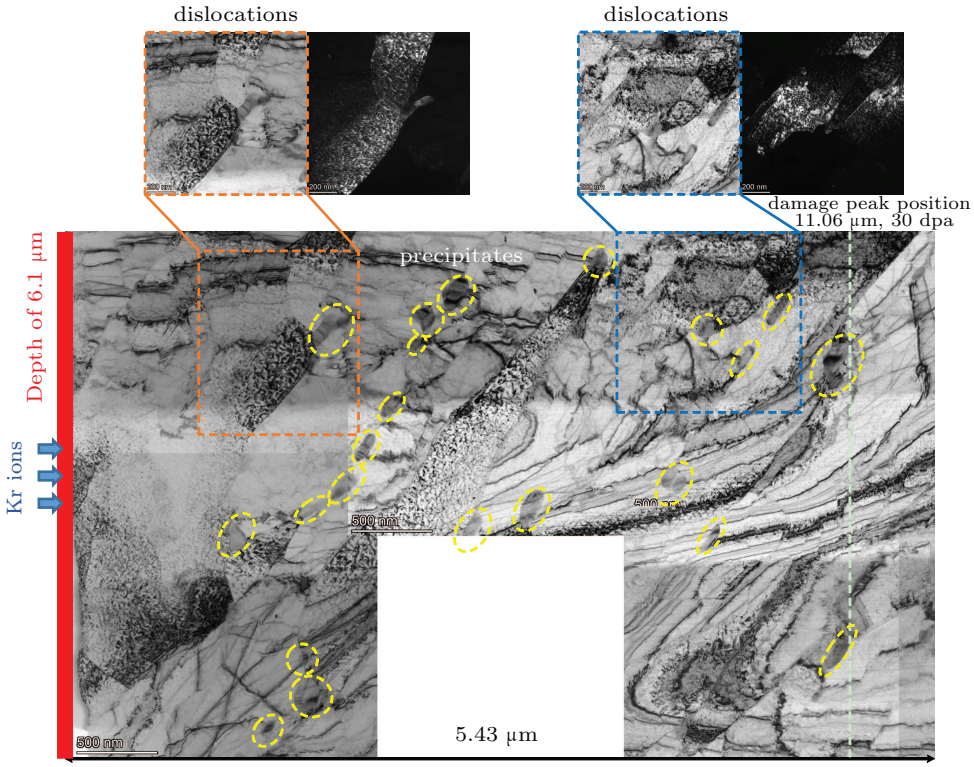


**Fig. 6.** TEM bright field image from 6.1 μm to ∼ 12 μm of T91 irradiated by $Kr^+$ ions. Two areas with dashed line are several characteristic morphologies in TEM bright field image and the corresponding dark field image are shown. The bright yellow dashed circle represents the precipitates. The white dashed line represents the damage peak position predicted by SRIM.

Three grains were selected for TEM analysis, as shown in Figs. 7(a), 7(d), and 7(g) located at the depth of 8539 nm, 9824 nm, 11421 nm with irradiation damages of 4.87 dpa, 10.48 dpa, 15.7 dpa, respectively. The selected area electron diffraction (SAED) results in Figs. 5 and 7 show that these selected areas have body-centered cubic (BCC) crystal structure. The crystalline interplanar spacing keep at ∼ 2.0 Å {200} or ∼ 1.4 Å {110}. Interestingly, with the increasing irradiation damage from 0.63 dpa to 15.7 dpa, the crystal structure in these selected areas maintain integrity. Figures 7(b), 7(c), and figures 7(e), 7(f) and figures 7(g), 7(h) display the same region with different $\boldsymbol{g}$ vectors, respectively. In Fig. 7(b), the deformation degree of grain boundaries is higher than that in Fig. 5(i). The higher irradiation dose, the stronger the interaction between defects and grain boundaries is. Inside the grains shown in Figs. 7(e) and 7(h), there are many dislocation seg-

ments at 10.48 dpa, which becomes unevenly distributed dislocations and location loops at 15.7 dpa. Compared the difference between Figs. 7(h) and 7(i), the dislocation loops only appeared with $g = 1\bar{1}0$. Taller *et al.*[24] found that very few $a_0/2\langle 111\rangle$ dislocation less than 10% of the total loop number density loops were observed between 432 °C and 460 °C with 16.6 dpa. At the higher temperatures of 510 °C:16.6 dpa and 520 °C:14.6 dpa, very few dislocation loops were observed. At the highest temperature of 570 °C:15.4 dpa, only dislocation lines were observed. In this study, the most of dislocation loops would be $a_0\langle 100\rangle$ type at high-dose region. But there are few dislocation loops present in grains. Instead, a large number of dislocation lines appear near grain boundaries.

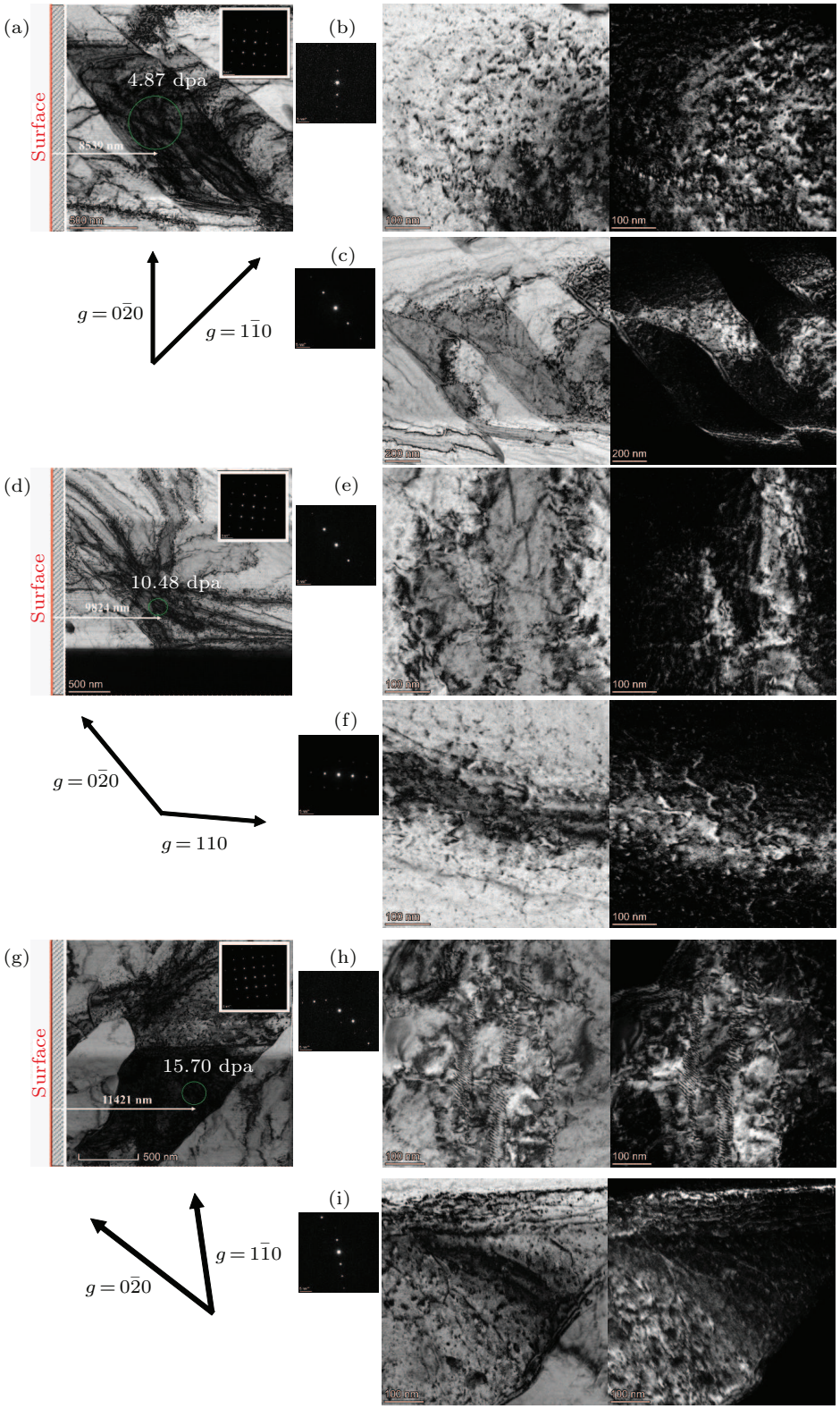


**Fig. 7.** Bright field and dark field TEM images of three grains with different $\boldsymbol{g}$ vectors from 6.1 μm to ∼ 12 μm of T91 irradiated by $Kr^+$ ions.

In this study, the microstructures of T91 irradiated by $Kr^+$ ions from surface to $\sim$ 12 μm have been investigated. The average size and density of precipitates in both the low-dose area from surface to $\sim$ 6 μm and the high-dose area from 6.1 μm to $\sim$ 12 μm are larger than those in origin T91 steel. Moreover, most precipitates are distributed near grain boundaries. As for the black dots, both the number density and average size of black dots in the low-dose area are larger than those of origin T91 steel. The elevated temperature and high irradiation damage would promote the migration and growth of small size defects such as black dots.

With higher irradiation damage from 1.76 dpa to 30 dpa, there are higher density dislocations in some grains, especially in the martensite laths. The high density dislocations become more unevenly distributed. Interestingly, the distribution of dislocations is closely related to grain boundaries. For the examined regions regardless of depth in T91 steel, the density of dislocations is usually at a high level when close to the grain boundary. The grain boundaries can act as strong sinks for irradiation defects. In T91 steel, the abundance of martensite laths provides this type of sinks for defects. Moreover, elevated temperature would make contribution to the migration of defects, which causes a large number of defects to accumulate near grain boundaries, especially in martensite laths. Also, the distribution of $a_0/2\langle 111\rangle$ or $a_0\langle 100\rangle$ dislocation loops is related to the migration. The $a_0/2\langle 111\rangle$ loops can migrate over long distances and interact with defects, whereas $a_0\langle 100\rangle$ can only act as stationary defect sinks once formed.[18] Furthermore, at elevated temperature, carbon atoms, acting as trapping sites for the loops, predominantly diffuse to line dislocations present at the martensite lath boundaries in the ferritic/martensitic steel.[25] And the dislocation loops are few due to the annealing effect, more vacancies migrate and annihilate at defect sinks including interstitials, dislocations, dislocation loops, grain boundaries, and precipitates.[16] Moreover, by atomistic simulations, Xu *et al.*[23] found that the formation of $\langle 100\rangle$ loops involved a distinct atomistic interaction between two $1/2\langle 111\rangle$ loops, and did not follow the conventional assumption of dislocation theory, *i.e.*, Burgers vector conservation between the reactants and the product. Therefore, the rest dislocation loops existing in the grains is mainly $a_0\langle 100\rangle$ type and large amounts of dislocation loops interact with other defects or carbon atoms, leading to the production of the dislocation segments. In addition, the $Kr^+$ ion irradiation enhanced the growth of precipitates such as carbide precipitation. The carbide precipitations on the prior austenite grain boundaries would contribute to the prolongation of recovery of martensite laths, as reported previously.[22] At 550 °C, the martensite laths still existed in the bulk material and made contribution to the suppression of irradiation defects in this study.

## 4. Conclusion

In summary, the microstructures of T91 steel irradiated by 196-MeV $Kr^+$ ions at 550 °C have been studied by TEM analysis. The following conclusions have been obtained.

(i) A large number of defects accumulated near grain boundaries in the whole irradiated area, especially in the high-dose area, which can be attributed to the abundance of martensite laths. The grain boundaries provided by martensite laths can act as strong sinks for irradiated defects.

(ii) At 550 °C, the migration of defects was significantly enhanced and a large number of defects accumulated near grain boundaries, especially in the martensite laths. When the large amounts of dislocation loops interacted with other defects or carbon atoms, it led to the production of dislocation segments. With increasing dose, the defects gradually changed from black dots to dislocation loops, and further formed dislocation walls near grain boundaries due to the production of a large number of dislocations

(iii) The dislocation loops are mainly $a_0\langle 100\rangle$ type in T91 irradiated by $Kr^+$ ions at 550 °C. The migration ability of $a_0/2\langle 111\rangle$ loops was higher than that of $a_0\langle 100\rangle$ and could operate over longer distances and interact with defects. Elevated temperature promoted more vacancies migration and annihilation at defect sinks including interstitials, dislocations, dislocation loops, grain boundaries, and precipitates. Therefore, $a_0/2\langle 111\rangle$ loops were incapable of stable existence but $a_0\langle 100\rangle$ loops would be remained in the bulk.

(iv) The $Kr^+$ ion irradiation enhanced the nucleation and growth of precipitates such as carbide precipitation. Interestingly, in the high-dose area, the density of precipitates was larger than that in the low-dose area but the size showed the opposite trend. The density and size of precipitates in both the high-dose area and the low-dose area were larger than those in the origin T91 steel.

## References


[1] Prasitthipayong A, Frazer D, Kareer A, Abad M D, Garner A, Joni B, Ungar T, Ribarik G, Preuss M, Balogh L, Tumey S J, Minor A M and Hosemann P 2018 *Nuclear Materials and Energy* **16** 34

[2] Zeman A, Debarberis L, Kocik J, Slugen V and Keilova E 2007 *J. Nucl. Mater.* **362** 259

[3] Horowitz E 2008 *Icone 16: Proceeding of the 16th International Conference on Nuclear Engineering* **4** 405

[4] Hahner P and Hurst R 2009 *Creep & Fracture in High Temperature Components: Design & Life Assessment Issues, Proceedings* 112

[5] Taller S and Was G S 2020 *Acta Materialia* **198** 47

[6] Gigax J G, Kim H, Chen T Y, Garner F A and Shao L 2017 *Acta Materialia* **132** 395

[7] Gigax J G, Chen T, Kim H, Wang J, Price L M, Aydogan E, Maloy S A, Schreiber D K, Toloczko M B, Garner F A and Shao L 2016 *J. Nucl. Mater.* **482** 257

[8] Getto E, Sun K, Monterrosa A M, Jiao Z, Hackett M J and Was G S 2016 *J. Nucl. Mater.* **480** 159

[9] Li B S, Wang Z G, Wei K F, Shen T L, Yao C F, Zhang H P, Sheng Y B, Lu X R, Xiong A L and Han W T 2019 *Fusion Engineering and Design* **142** 6

[10] Xu C and Was G S 2013 *J. Nucl. Mater.* **441** 681
[11] Yeli G M, Strutt V C I, Auger M A, Bagot P A J and Moody M P 2021 *J. Nucl. Mater.* **543**
[12] Van Renterghem W, Terentyev D and Konstantinovic M J 2018 *J. Nucl. Mater.* **506** 43
[13] Jiao Z, Taller S, Field K, Yeli G, Moody M P and Was G S 2018 *J. Nucl. Mater.* **504** 122
[14] Tan L, Kim B K, Yang Y, Field K G, Gray S and Li M 2017 *J. Nucl. Mater.* **493** 12
[15] Zhu H P, Hao Z L, Shen T L, Cui M H, Fang X S, Wang Z G, Niu F L, Zhao Y G, Yang A X and Zhang Y 2017 *Fusion Engineering and Design* **125** 372
[16] Zhu H P, Wang Z G, Cui M H, Li B S, Gao X, Sun J R, Yao C F, Wei K F, Shen T L, Pang L L, Zhu Y B, Li Y F, Wang J and Xie E Q 2015 *Appl. Surf. Sci.* **326** 1
[17] Zheng C and Kaoumi D 2020 *J. Nucl. Mater.* **540** 9
[18] Liu X, Miao Y B, Li M M, Kirk M A, Maloy S A and Stubbins J F 2017 *J. Nucl. Mater.* **490** 305
[19] Biersack J P and Ziegler J F 1984 *Ion Implantation Science and Technology* **1** 51
[20] Kumar N N, Tewari R, Mukherjee P, Gayathri N, Durgaprasad P V, Taki G S, Krishna J B M, Sinha A K, Pant P, Revally A K, Dutta B K and Dey G K 2017 *Radiation Effects and Defects in Solids* **172** 678
[21] Jiao Z J, Shankar V and Was G S 2011 *J. Nucl. Mater.* **419** 52
[22] Yamashita S, Yano Y, Tachi Y and Akasaka N 2009 *J. Nucl. Mater.* **386–388** 135
[23] Xu H X, Stoller R E, Osetsky Y N and Terentyev D 2013 *Phys. Rev. Lett.* **110** 265503
[24] Taller S, Jiao Z J, Field K and Was G S 2019 *J. Nucl. Mater.* **527** 151831
[25] Dutta A, Gayathri N, Mukherjee P, Dey S, Mandal S, Roy T K, Sarkar A, Neogy S and Sagdeo A 2019 *J. Nucl. Mater.* **514** 161